Title

Monitoring of bearing failure in composite bolted connections using ultrasonic guided waves: A parametric study

Journal

Structural Health Monitoring, 13(1)

ISSN

1475-9217

Authors

Haynes, Colin
Todd, Michael
Nadabe, Takeaki
et al.

Publication Date

2014

DOI

10.1177/1475921713510756

Peer reviewed

Monitoring of bearing failure in composite bolted connections using ultrasonic guided waves: a parametric study

Colin Haynes[1], Michael Todd[1], Takeaki Nadabe[2], Nobuo Takeda[2]

ABSTRACT

Bearing damage in composite bolted connections (such as those commonly used in aerospace applications) is investigated through the application of ultrasonic guided waves. Specifically, identical macro fiber composite sensor arrays were bonded to each of two identical composite plates. One plate was then inspected ultrasonically in the unloaded condition with bearing damage being introduced through successive uniaxial tensile tests, while the other plate was assessed while under load in the tensile testing machine. A scattering matrix approach is employed to characterize the interaction of the guided waves with the target bolt hole. The effects of applied load and the bolt fixture on the ultrasonic results are explored. A parametric study is carried out to determine the optimal actuation frequency and interrogation angle for this application. The results demonstrate that the system is capable of detecting bolt bearing damage as well as monitoring of the applied load in the elastic region.

KEYWORDS

CFRP, MFC, Ultrasonic Guided Waves, Load Dependence, Bolt Bearing Failure

INTRODUCTION

In recent years, carbon fiber reinforced polymer (CFRP) composite materials have become a material of choice in the aerospace industry due their high specific strength and stiffness properties. Transitioning to this relatively new material poses challenges, however, especially in the area of connection design. Mechanically-fastened connections, and particularly bolted joints, are currently the most common connection type for CFRP primary structures. Special care must be taken in the design process of these connections due to the brittleness of composite material and the possibility of high stress concentrations due to anisotropy.[1] Recent advances have been made in characterizing the failure modes of CFRP bolted connections, but this remains an active research area.[2,3] In this study, bearing failure of CFRP bolted joints is chosen as the focus, primarily because connections that fail in this mode tend to have the highest strength.[4]

It is becoming increasingly important, therefore, to begin to develop systems capable of monitoring the failure mechanisms of such structures. Structural health monitoring (SHM) is a field concerned with assessing the condition of a structure through continuous, on-line, non-destructive measurements and appropriate data processing. In particular, ultrasonic guided waves (UGWs) have become an attractive and increasingly popular technology for SHM

[1] Department of Structural Engineering, University of California - San Diego, La Jolla, CA 92093 USA
[2] Dept. of Advanced Energy, University of Tokyo, Mail Box 311, 5-1-5 Kashiwanoha, Kashiwa-shi, Chiba, 277-8561 Japan

Corresponding author:
Corresponding Author: Michael Todd, Email: mdtodd@ucsd.edu, Tel: 858-534-5951

because they combine relatively high sensitivity to local damage with relatively long inspection ranges.[5] Some work has been done to analyze bolted joints with UGWs in the past, typically in isotropic, metallic test articles. Doyle et al. implemented UGW inspection for monitoring of bolted space structures, demonstrating that small phase shifts occur with the loss of bolt torque.[6] As an extension of that work, Zagrai et al. quantified the acoustoelastic effect in the aluminum structure and proposed a baseline-free methodology for detection of bolt loosening.[7] Lee et al. compared the mildly anisotropic effect of applied loads on an aluminum structure and compared these changes to those produced by temperature variations.[8] Furthermore, Chen et al. proposed taking advantage of load variations opening and closing fatigue cracks to perform baseline-free detection and localization.[9] Guided waves and the acoustoelastic effect have also been used to nondestructively evaluate bolt torque levels directly.[10]

The objective of this study is to characterize experimentally the interaction of Lamb waves with bolt bearing damage in CFRP bolted joints and to determine the viability of detecting such damage using macro fiber composite (MFC) sensor-actuators. This work advances the field by considering the challenge of monitoring bolted joints in composite materials while under uniaxial load for the initiation of a complex failure mode. While work has been done in isotropic materials to quantify the interaction of guided waves with scatterers, other researchers have examined the effect of load on guided waves in isotropic materials, and yet others have proposed inspecting bolted joints with ultrasonic guided waves, to the authors' knowledge this is the first study monitoring bolt damage in CFRP materials using guided waves, particularly in the presence of load variations. As such, it is reasonable and valid to take an empirical approach in order to characterize the physical phenomena that arise in this unique test condition. Specific emphasis is placed on the directionality of the guided wave interaction as well as a study of the relevant parameters for damage detection. To that end, two CFRP test specimens were fabricated and loaded to induce bolt bearing failure while ultrasonic measurements were periodically taken for inspection. Experiments were carried out to determine the frequency of actuation and interrogation angles that are most effective for damage detection, as well as to investigate the effect of applied load on the detection problem.

EXPERIMENTAL PROCEDURE

Test Specimens

In order to experimentally investigate the interaction of guided waves with bolt bearing damage, two CFRP test specimens (referred to as plates 101 and 102) were fabricated. The laminates consisted of eight T700S/2592 prepreg layers in a $[-45\ 0\ 45\ 90]_s$ stacking sequence. The final laminate measured 200 mm x 120 mm x 1.15 mm with 6-mm-diameter holes drilled to accommodate the tensile testing equipment. This test fixture is shown in Figure 1. The contact pressure from the bolted connection on the target hole is concentrated in 40-mm-square CFRP washers on either side of the plate, which allow the other connecting elements to grip the specimen without contacting any of the MFC sensors. The testing configuration puts the highest stress on a single target hole in a double shear configuration, ultimately introducing bolt bearing failure.

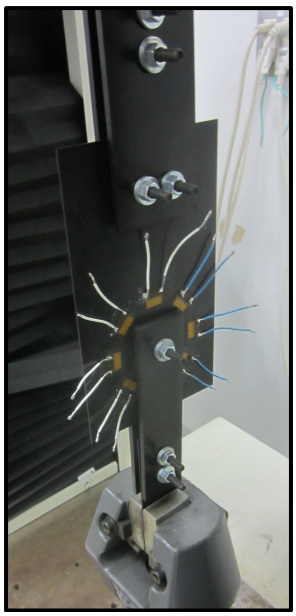

Figure 1 - Plate 101 in the tensile testing apparatus at the Univ. of Tokyo

Data Acquisition and Feature Extraction

Both test specimens were instrumented with a uniformly-spaced circular array of eight MFCs, each a M2814-P2 type cut to a final dimension of 14 mm wide by 6 mm long. These sensors were bonded to the surface of the laminate with a standard two-part epoxy adhesive 30 mm away from the center of the target hole. MFCs are favored in composite applications because of their conformability to curved surfaces, their directional actuation characteristics, and their durability. Other studies have demonstrated the usefulness of MFCs in guided wave SHM for such applications.[11,12] By positioning the MFCs in a uniform circular array around the target hole (about which the defect was introduced), a scattering matrix approach may be utilized to determine the optimal angles of interrogation. Essentially, this approach involves measuring the amplitude of the response to guided wave scatter in different directions in order to quantify the interaction of such waves with the target defect.[13] The advantage of using the circular array is that it allows a number of different interrogation angles to be tested easily.

Tests were run using each MFC to actuate sequentially, each time receiving with all other sensors. The actuation signal was chosen as a three-cycle Gaussian modulated sinusoid. Generally, the optimal frequency for actuation of a UGW SHM system is a function of the sensor properties and the ratio of the defect size to the wavelength. While determining the amplitudes and directions of the guided wave modes generated by an MFC sensor is complicated, Collet et al. have presented some information obtained from finite element analysis.[14] From this information, it may be inferred that the forward-propagation direction (the wave that will interact with the bolt hole) is dominated by the S_0 mode of propagation. However, this study is not focused on such specific modal analysis of the wave propagation—rather, it is focused upon empirically finding the parameters which provide the best performance. For plate 101, a center frequency of 300 kHz was chosen because it provided a relatively high-amplitude response for the forward-propagating wave. Likewise, rather than calculating the dispersion curves for this particular anisotropic CFRP layup, the velocity of the dominant mode was determined from a simple experiment in a feature-less plate of the same material. Bonding two identical MFC sensors 60 mm apart on the surrogate plate, the same actuation parameters were used to launch and receive a pulse. From a basic time-of-flight calculation, the velocity was found to be about 4000 m/s. The data acquisition system used for plate 101 did not support pulse-echo measurements and sampled at 10 MHz.

Plate 102, however, was tested with a different data acquisition system, enabling a more detailed study of the optimal frequency to be undertaken (which will be presented later). The second data acquisition system sampled at 2.5 MHz while permitting the measurement of pulse-echo responses.

To process each waveform, first a band-matched filter is applied by convolving the received signal with the input signal and then enveloped by taking the magnitude of the Hilbert transform of the signal. This filtering procedure has the effect of eliminating frequency content other than the frequency content from the actuation (that is, assuming linear data acquisition). Given that the sensor locations and wave speed are known, it is straightforward to determine the time window inside which the direct arrival mode should fall. The other arrivals are either insensitive to damage (because the path does not interact with the hole) or more sensitive to non-damage-related parameters (because the path includes edge reflections). For this reason, the data are windowed in time to select only the proper wave packet, with the same window being used for all sensor pairs (since the nominal distances are the same and velocity differences are minimal). Because no model for the effect of bolt bearing damage on guided waves in composites is available, it is difficult to determine an optimal detector *a priori.* Therefore, the normalized residual energy is used, defined as

$$\text{Normalized Residual Energy} = \frac{\sum_{n=t_0}^{t_f} \mathbf{x}[n]^2}{\sum_{n=t_0}^{t_f} \mathbf{y}[n]^2}, \tag{1}$$

where **x** represents the residual signal after baseline subtraction, **y** is the corresponding baseline signal, n is the sample index, t_0 is the start time of the window, and t_f is the end time of the window. Note that the baseline subtraction technique (elaborated upon in the following section) is applied to the RF signal, prior to the enveloping and time-windowing procedures. This technique was presented previously by the authors as an optimal solution to some guided-wave applications when other information about the system-under-test is minimal.[15]

Damage Introduced

Each specimen was tested destructively to three different damage levels. The first level corresponded to the first load drop observed in during the displacement-controlled tensile test and the following two damage levels were based on a prescribed displacement after the initial load drop. However, the two plates used a slightly different procedure. Tests for plate 101 were conducted at the University of Tokyo. For this specimen, the damage was introduced across multiple tests, with the specimen unloaded and removed from the bolt fixture for the ultrasonic interrogation between each stage (in this way, the plate boundary conditions were kept consistent). The damage in plate 102, by contrast, was introduced at the University of California, San Diego by a single tensile test, where the loading was merely paused with current static load level maintained to take ultrasonic readings. Because the most of the tests were conducted without removing the bolt fixture, the lateral restraint condition remained consistent, although necessarily different from the plate 101 condition. Figure 2 and Figure 3 show the load-displacement curves for each of the tests conducted. During the pauses at the discrete loading levels for plate 102, the test specimen relaxed slightly, causing the load drops for a constant displacement that can be seen at regular intervals (particularly at higher load values). However, the ultrasonic interrogation was not performed until the load level was stable enough (relative to the load increment of the tensile test) for all sensors to take their readings at the same nominal load.

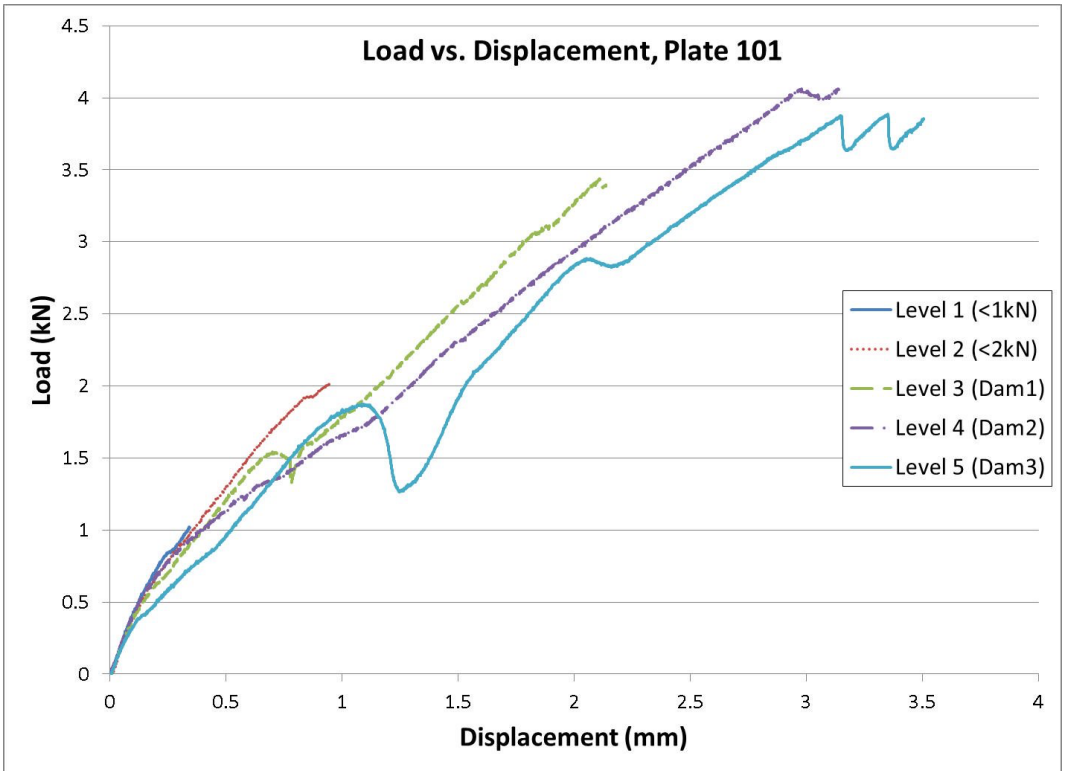

Figure 2 - Load-displacement curve for plate 101 tests (Univ. of Tokyo)

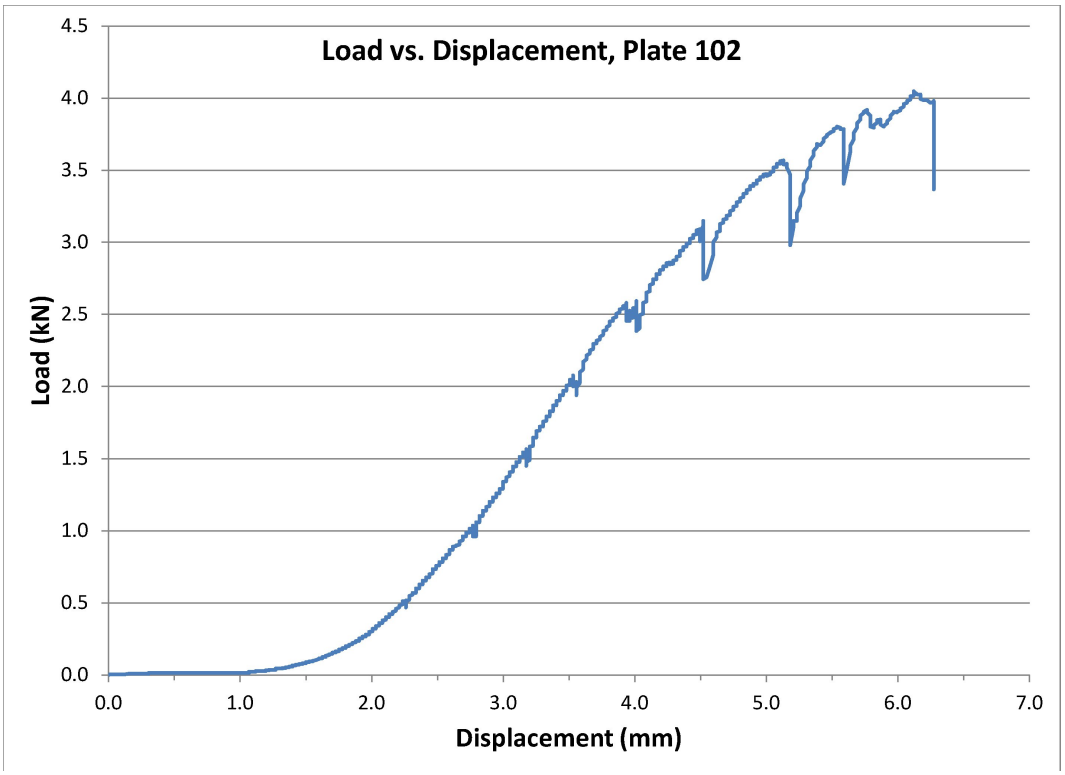

Figure 3 - Load-displacement curves for plate 102 tests (Univ. of Calif., San Diego)

Naturally, the specific structure of the bolt bearing damage is expected to differ slightly between each plate. Lateral clamping force and washer type have been shown to influence the structure of the damage and the stress level at which the damage initiates.[16] Figure 4 is a photograph of plate 101 after the highest level of damage was introduced. Following the test,

the specimen was cut and polished in order to capture the cross-section of the damage with an electron microscope – the result being presented in Figure 5. In particular, note the periodic buckling of the zero-degree fibers (second from outside) and the "X" patterns in the inner layers denoting shear failure.[3] This example of the damage microstructure is presented to provide a clearer picture of the type of damage that is being examined. The particular damage structure emerging for each specimen is not of primary importance, however, since an SHM system should be robust to slight changes of this sort.

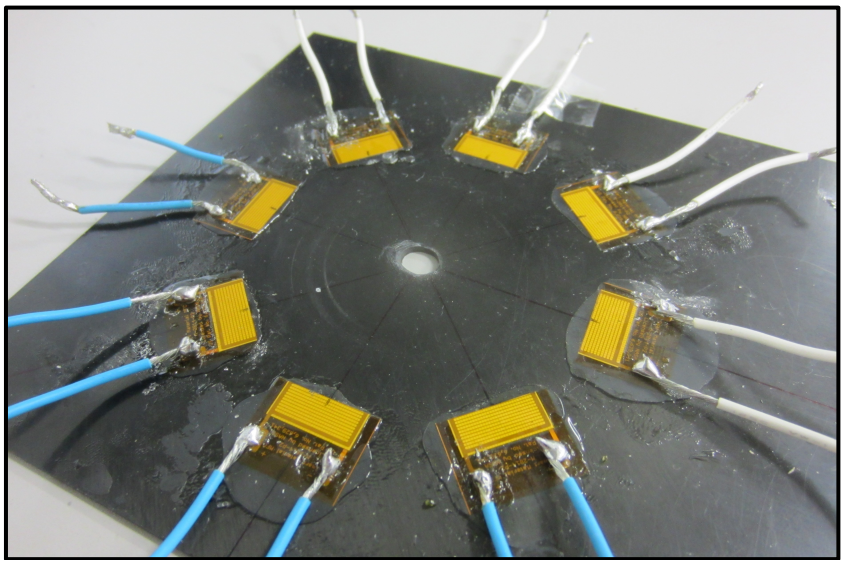

Figure 4 - Sensor layout for plate 101 (shown with highest damage level)

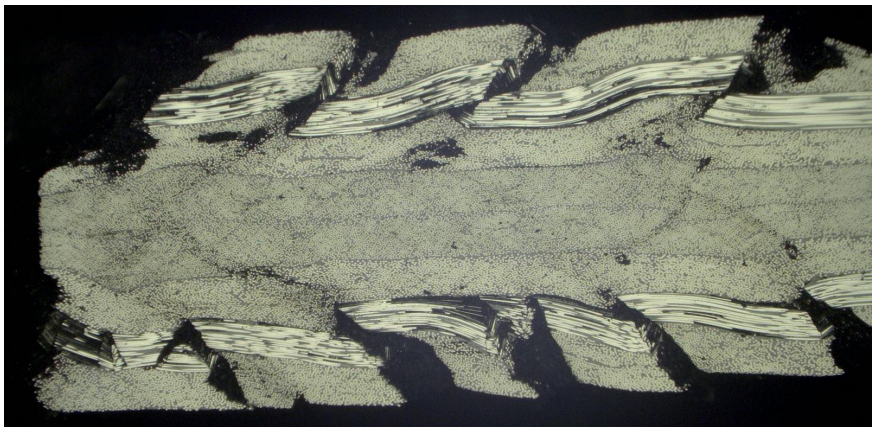

Figure 5 - Electron microscope picture of the cross-section of bearing damage in plate 101

In order to evaluate the sensitivity of the system to bolt bearing damage, an optimal baseline subtraction (OBS) scheme was implemented.[17] In this framework, a set of "baseline" measurements are collected from the structure in a reference (usually presumed to be undamaged) state. This set of baselines should span the range of operating conditions the structure is expected to see. When a new measurement is made, the "closest" baseline (as measured by some norm) is subtracted from it, resulting in a residual waveform that should be minimized for an undamaged state while increasing in magnitude when damage is introduced. Again, the OBS procedure is performed on the RF signals prior to any windowing procedures to ensure the most accurate compensation, and because the specimen is assumed to be at one environmental state, the norm is computed across all sensor pairs together. While this method was developed in the context of temperature compensation, the

algorithmic procedure is quite general and can be used to compensate for any types of variability, including load state, contained within the baseline set. For plate 101, three baseline measurements—meaning a full series of tests so that each sensor actuates in turn while every other sensor receives—were taken before loading. Then three measurements were taken after each of the five load levels (two in the elastic region and three progressive levels of damage). For plate 102, 18 test sets were taken before any loading in various configurations (the specimen being placed in and removed from the bolt fixture). A baseline tensile test was then conducted to 2 kN (remaining within the elastic region) with two baselines taken at every 0.5 kN interval. Finally, two measurements were taken at 0.5 kN intervals in the main tensile test (shown in Figure 3), composing the undamaged data and three levels of damaged data, with eight additional unloaded cases recorded after the damage had been introduced.

EXPERIMENTAL RESULTS

A representative group of waveforms is shown in Figure 6. The figure gives all of the waveforms recorded by the 6-7 sensor pair over the course of the final tensile test after the filtering and envelope procedures. As such, the load is increasing for subsequent waveforms leading to the introduction of damage at the end of the test. The green vertical lines denote the boundaries of the time window used to isolate the wave packet of the dominant mode that interacts with the target hole. The wave packet around 10 μs is the result of the directional profile of the MFCs, which causes some energy to travel directly between adjacent sensors, thus arriving earlier than the intended first arrival. Arrivals at 30 μs and later represent reflections from the boundaries of the relatively small plate. Inspection of the peak of the wave packet of interest, as shown in the inset of Figure 6, reveal that the amplitudes vary both with load and with damage level. This phenomenon will be addressed in a later section.

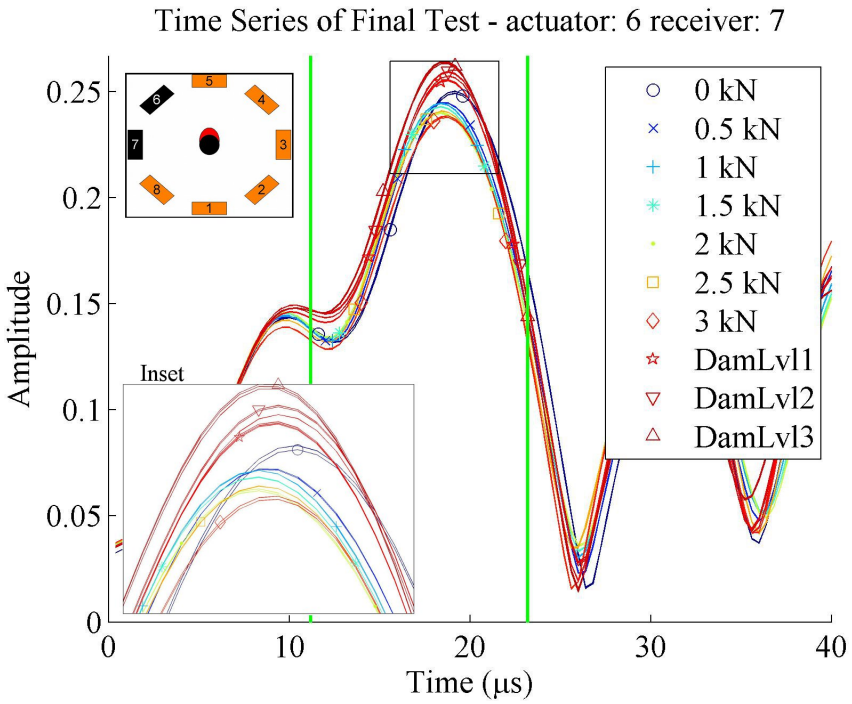

Figure 6 - Enveloped and filtered time series results for final tensile test of plate 102 (backscatter angle)

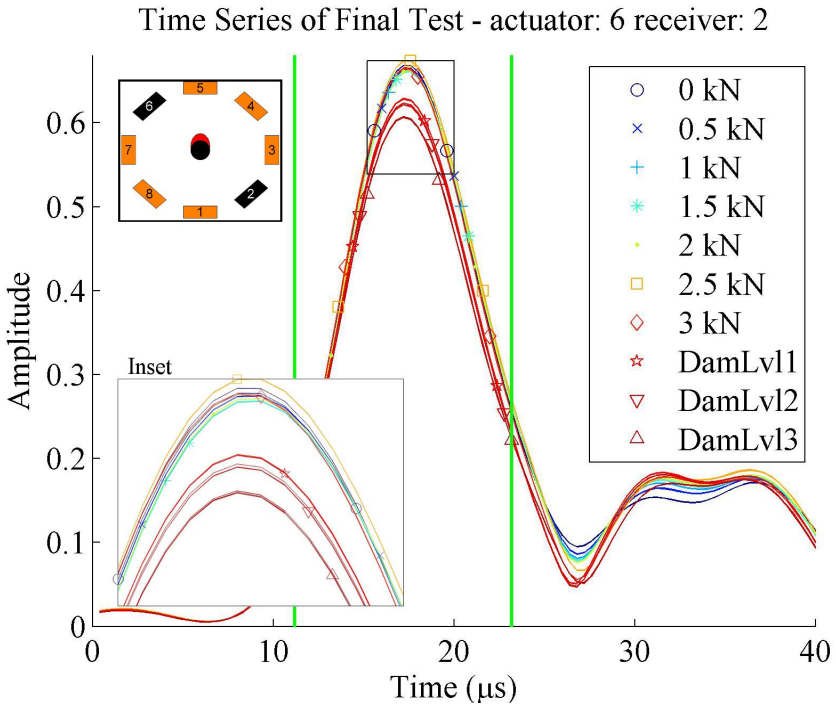

Figure 7 - Enveloped and filtered time series result for final tensile test of plate 102 (through-transmission angle)

Scattering matrix approach

Any change in the mechanical impedance of a structure, due to features such as defects or material/geometry changes, will cause elastic waves to scatter in a way that is governed by material properties, wave properties, and the specific geometry of the feature. A scattering matrix is one way of quantifying the magnitude and directionality of that interaction. Different authors may describe the phenomenon in different ways, as was succinctly summarized by Wilcox and Velichko.[13] Scattering matrix methods typically compare the magnitude or energy of the wavefront scattered in all directions for a given angle of incidence.[18] Usually these representations consider the far-field scattering behavior of the target feature.[13] Furthermore, most previous studies of scattering behavior have tended to focus on model-driven techniques, whereas this paper will present an experimental estimation of the scattering profile for the damage in both specimens. A more detailed scattering matrix analysis of plate 101 has been published previously.[19] For reflections from an undamaged circular hole, the scattering matrix result can be calculated theoretically (at least for isotropic materials) and determined analytically using techniques such as finite element modeling or semi-analytical finite element modeling.[20] However, such results are not readily available in the literature for anisotropic materials, and specifically not for defect structures like the one considered in this work.

First, one representative first-arrival-amplitude scatter plot is given for each specimen. Note that the angles are defined such that the damage propagates in the 180° direction. Each plot presents the results for only one actuator (labeled in the figure – all examples are given for sensor 4 or 135°) with each sensor's response plotted in the direction of that sensor. The plots for plate 102 also include pulse-echo channels, represented by the data points along the actuator direction. The amplitudes of these pulse-echo channels are more variable than the respective pitch-catch channels because they are significantly influenced by electro-magnetic interference effects due to the actuation. Despite this variability, some cases still showed statistical separation between damaged and undamaged cases, so the pulse-echo channels have been included in the analysis. Again, only the pulse-echo data are affected by this

problem – the vast majority of the data in this study were collected in the pitch-catch mode and the data acquisition in this mode is perfectly acceptable.

It is evident from the plate 101 results given in Figure 8 that the experimental scattering matrix result, even for the undamaged cases, is not symmetric. The plate 102 result (Figure 9) appears closer to a symmetric result, but it is also markedly asymmetric for certain other actuation angles. The quasi-isotropic laminate would only be expected to be slightly directional (as demonstrated by Salas and Cesnik[21]), and the results are not generally consistent with how the results for such a material would behave. The bolt fixture is unlikely to be the cause, since the plate 101 tests were conducted after removing the specimen from the bolt fixture (thus there was no contact around the bolt hole). Plate 102 tests were all taken without removing the specimen at all, meaning that the interaction was consistent over all tests, and because there is less asymmetry in the results of Figure 9, it is reasonable to conclude that lateral restraint is not likely the cause. Instead, discrepancies among sensors such as slight variations in location, orientation, and bond condition are probably the main factors contributing to the asymmetry. In both cases, it is difficult to determine any pattern relating to damage from the first-arrival-amplitude scattering matrix comparisons.

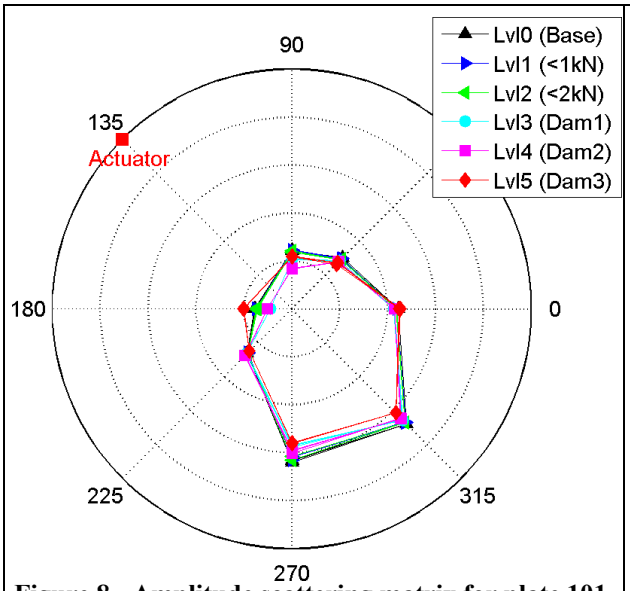

Figure 8 - Amplitude scattering matrix for plate 101, actuation at 135°

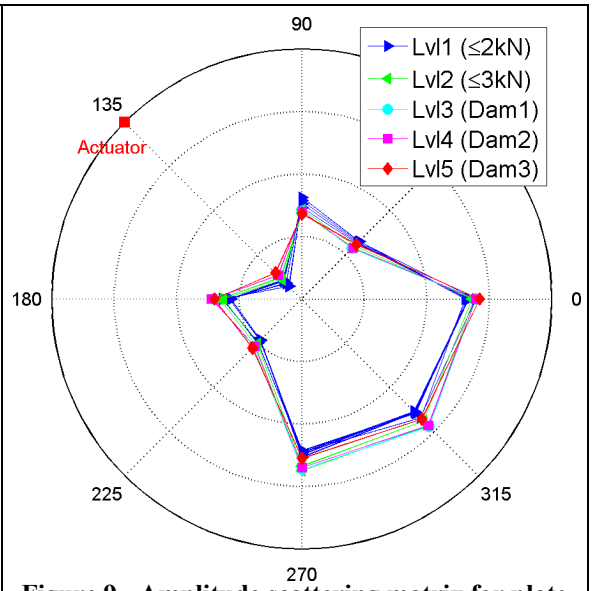

Figure 9 - Amplitude scattering matrix for plate 102, actuation at 135°

Baseline Subtraction

To visualize the damage progression another way, the normalized residual energy metric described in equation (1) is used to construct scattering matrices. The resulting values are converted to decibels; then, because the dB values are negative (which is inconvenient for polar plots), the minimum value (across all sensors and trials) is subtracted. This procedure results in values where the smallest magnitude corresponds to the smallest deviation from the baseline and the radial axis is in dB units. As a result, the plots shown are qualitative in nature, meant to highlight the patterns of residual scatter with the angle of interrogation.

First, it is clear from the baseline subtracted results that increasing damage level produces an increase in residual energy, which is particularly pronounced (i.e., there is considerable distinction among each damage level) for certain angles and not as clear for others. Comparing the results for the two specimens against one another, however, the results are qualitatively quite dissimilar. As demonstrated by Figure 10 for plate 101, the reflections

scattering back from the damaged side of the hole produce a very good statistical discrimination among damage cases. However, the result from plate 102 shown in Figure 11 suggests the opposite – receiving on the opposite side of the hole from the actuator produces the best discrimination. In the next section, this will be investigated more quantitatively and a possible cause of the discrepancy will be discussed.

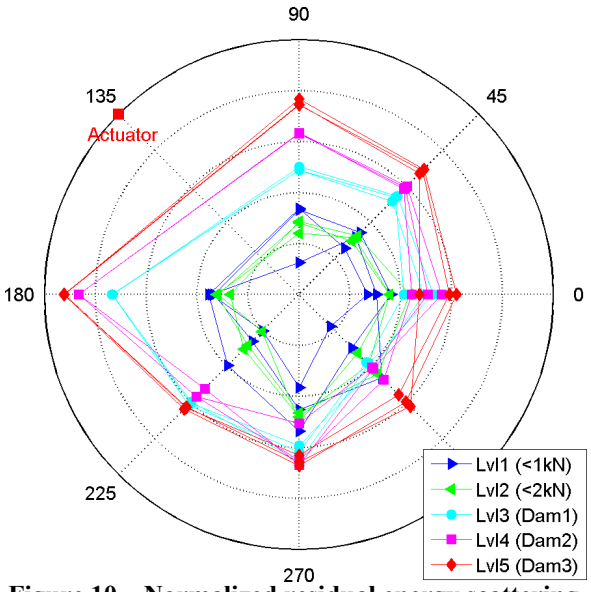

Figure 10 – Normalized residual energy scattering matrix for plate 101, actuation at 135°

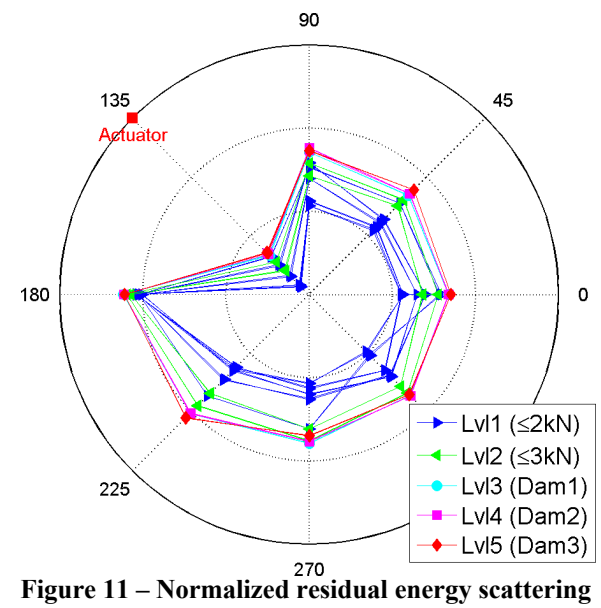

Figure 11 – Normalized residual energy scattering matrix for plate 102, actuation at 135°

Interrogation angle

For each sensor pair, the class separation between the data from each damage level and the undamaged data is computed. Because of the small sample sizes when considering each sensor pair and frequency independently (particularly for the damaged cases), it is difficult to estimate the intra-class variability accurately. Also, the normalized residual energy metric proposed is non-negative and should always increase as damage is introduced. Therefore, a modified version of the Student's t-test statistic is implemented as

$$\text{Modified Student's t-test statistic} = \sum_i \frac{d}{\sigma}, \qquad d = \begin{cases} x_i - \mu, & x - \mu > 0 \\ 0, & x - \mu < 0 \end{cases} \tag{2}$$

where σ is the standard deviation of the undamaged class, μ is the mean of the undamaged class, and x_i represents each metric value for the damaged class. Note that the difference is set to zero if the sample value is less than the mean of the undamaged class. It should be emphasized that the class separation metric is not intended to be used for detection, but is instead used to compare various acquisition parameters given knowledge of the class labels for each test.

Figure 12 (which is taken from plate 101 data) shows the class separation for each of the three damage levels. It should be noted that the very high values of the distance measure occur because there is excellent separation among classes for specific sensor pairs. Ultimately, the scale of the vertical axis is not important, as these comparisons are designed to show what interrogation angles are the most sensitive in a relative way. Utilizing the plots in this manner, it is evident that the best separation in each case is obtained by using the sensors on the damaged side of the hole (4, 5 and 6) both to actuate and to receive. That is,

the results are best when waves are launched from the damaged side so that they reflect off of the damage and are received by a nearby sensor – henceforth, the “backscatter angles”.

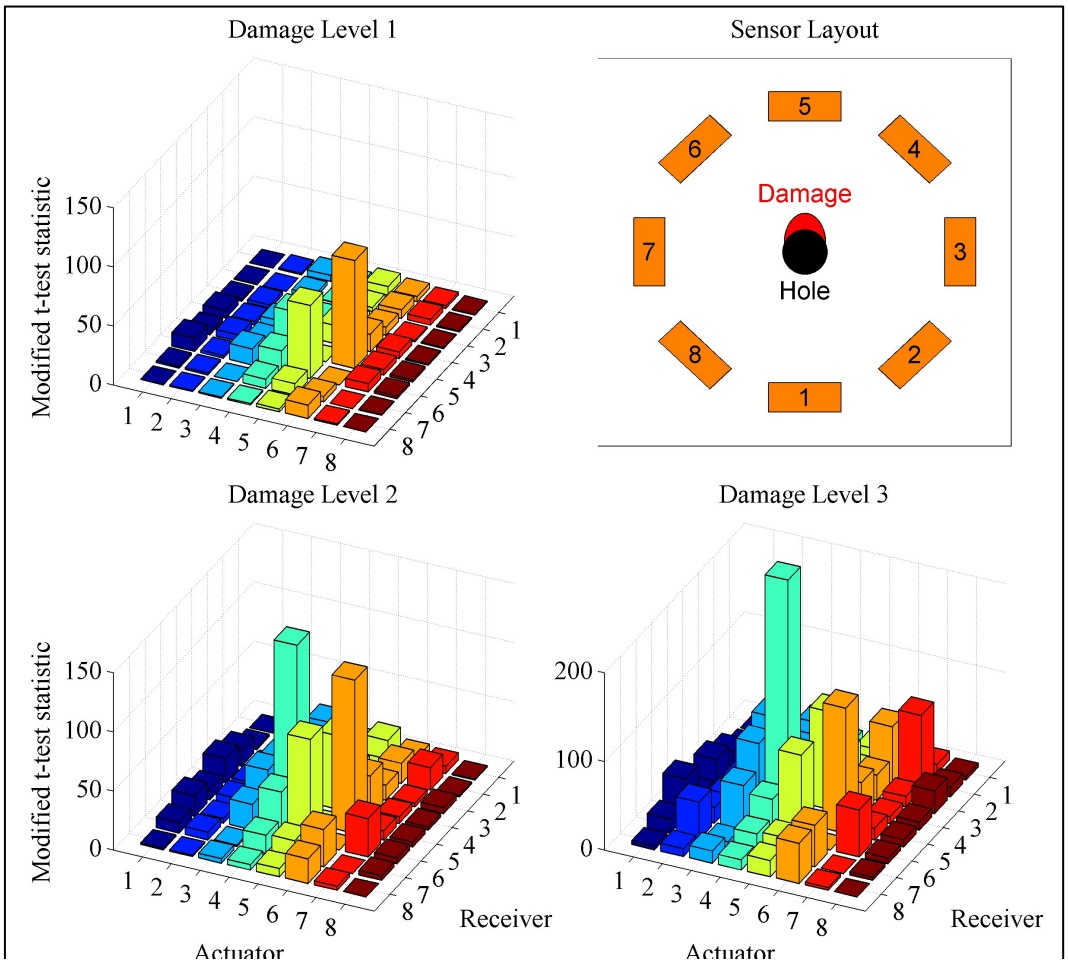

Figure 12 - Interrogation angle comparison for plate 101 (actuation frequency = 300 kHz)

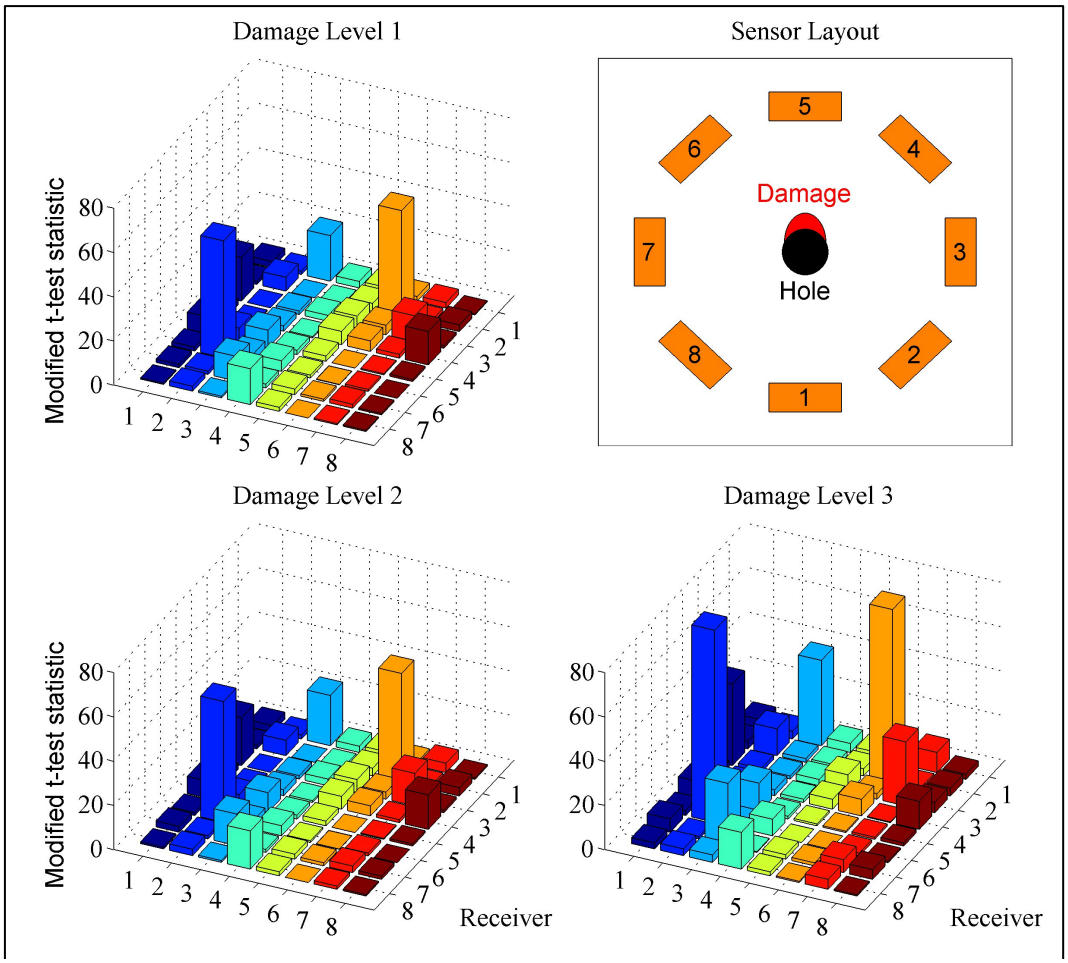

Figure 13 - Interrogation angle comparison for plate 102 (actuation frequency = 300 kHz)

Figure 13 shows the analogous data for plate 102, using only the 300 kHz data for consistency. In this case, however, the pattern is not the same. Instead of the damaged side of the hole being most preferred for actuating and receiving, the plate 102 data suggest that the through-transmission paths (the sensors separated by 180 degrees) are the optimal choice for detecting the damage. Because the plates were fabricated and instrumented according to an identical procedure, the most likely cause for the dramatic difference is that the measurements from plate 102 were taken under load, while the plate 101 tests were always conducted with the load removed. The loading seems to cause the bolt and bolt fixture to interact with the plate differently, resulting a different pattern. This hypothesis was confirmed by comparing results from plate 102 taken before and after the introduction of damage with the specimen removed from the bolt fixture. The resulting comparison is given in Figure 14, and the trend is much more similar to the plate 101 results than to the plate 102 results obtained under load. Utilizing typical modeling approaches to predicting the scattering from defects such as presented by Fromme and Sayir,[20] such influences may be difficult to predict in advance, underscoring the reason an empirical approach was implemented here. Of course, the situation in practice may be different as well, since most connections involve more bolts than just one as well as more complex contact conditions. These considerations, while worthy of further study, are beyond the scope of this study.

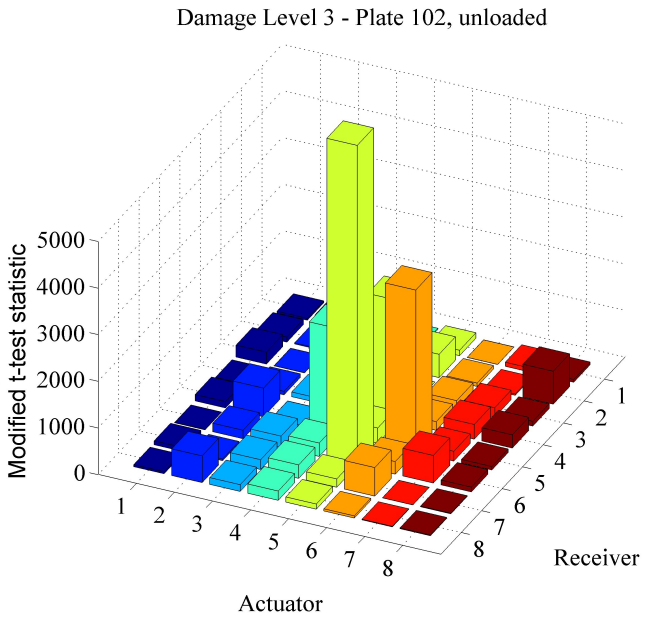

Figure 14 - Interrogation angle comparison for plate 102, unloaded, no bolt fixture

Optimal actuation frequency

Using the same modified t-test metric as in the interrogation angle comparison over the average of the normalized residual energy levels of all sensor pairs, the effect of actuation frequency was studied for the plate 102 data. The results are given in Figure 15, where the class separation values for each damage level (1-3) are stacked on one another. These results imply that there is a peak in system performance around 325 kHz. The trend in Figure 15 is quite similar to the trend in the observed actuation amplitude (which is dependent primarily on the sensor properties). That higher signal amplitude would facilitate better detection performance is not surprising. On the other hand, the wavelength of the interrogation signal in this case varies between approximately 2.5-6 mm or about 0.4 to 1 hole-diameters. It is interesting that in this case, the effect of signal amplitude seems to be more important than any sensitivity gained by matching the wavelength more closely with the damage scale. Ultimately, this comparison confirms that the 300 kHz actuation frequency selected for previous comparisons is nearly optimal for the SHM system considered here.

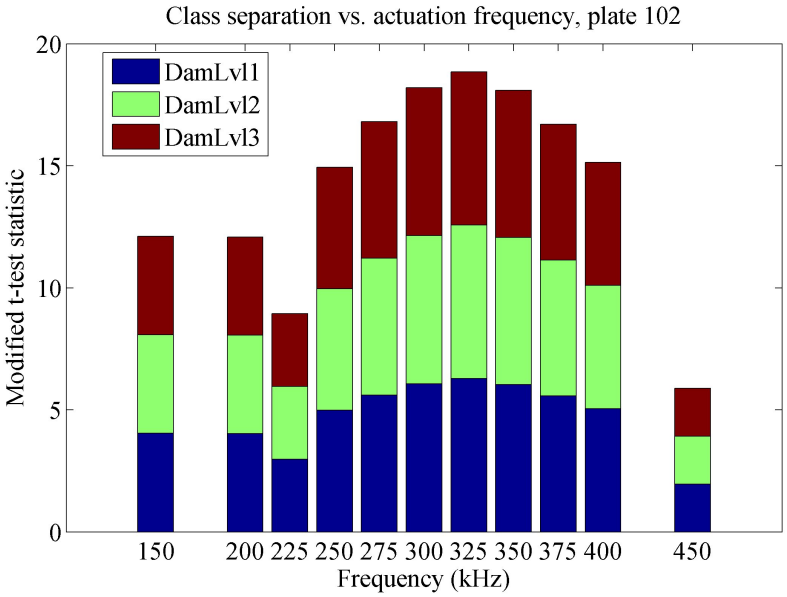

Figure 15 - Actuation frequency comparison for plate 102

Applied load

The tests conducted on plate 102 included the effect of applied load, with the majority of the tests being conducted without removing the specimen from the tensile testing machine. It has been shown that applied stress on a material has a nonlinear and anisotropic effect on wave propagation, known as the acoustoelastic effect. This change causes a very slight shift in both the group and phase velocity of the wave; measured in all directions for a unidirectional CFRP laminate, one study found the maximum velocity change to be around 1.9×10^{-4} /MPa.[22] Using this value as an estimated upper bound on the acoustoelastic effect in CFRP, it can be shown that such a phase difference would be very difficult to measure accurately given the sampling rate of the present system and the small size of the specimen – full details of that calculation have been presented by Haynes and Todd.[23] Lee et al. do propose a way of finding small phase shifts through a zero-crossing method,[8] but such an estimation is impractical in this case due to the complicated stress state around the bolt hole and higher noise floors due to limitations on signal averaging. However, it has been noted in the plate 102 tests that a much more significant change is observed in the amplitude of the waves with increased load. This primary effect is most likely due to the interaction of the bolt itself with the guided waves, which can be reasonably assumed to change with load level.

Because there is a noticeable change in the received signals for different levels of load, it is necessary to compensate for those changes (or be able to identify and quantify them) in order to detect the formation of bolt bearing damage. The results show that it is possible to classify the low load levels from the load level of the baseline identified as being closest in the OBS procedure. This is, in effect, using a k-nearest neighbor classifier with k=1. In this way, load states within the allowable operating range can be monitored with this system (all undamaged records in the load range where baselines existed were assigned the correct load state by this procedure). For the higher loads for which baselines were not obtained, it would likely be more difficult in practice to obtain information for a supervised learning approach, but the system as implemented now does show an increase in the residual level, which, given proper threshold selection, would provide warning that the load exceeds the maximum allowable. Of course, this procedure would become more difficult if the load state was more complex than the current uniaxial condition – however, for the present case, this compensation method proves effective.

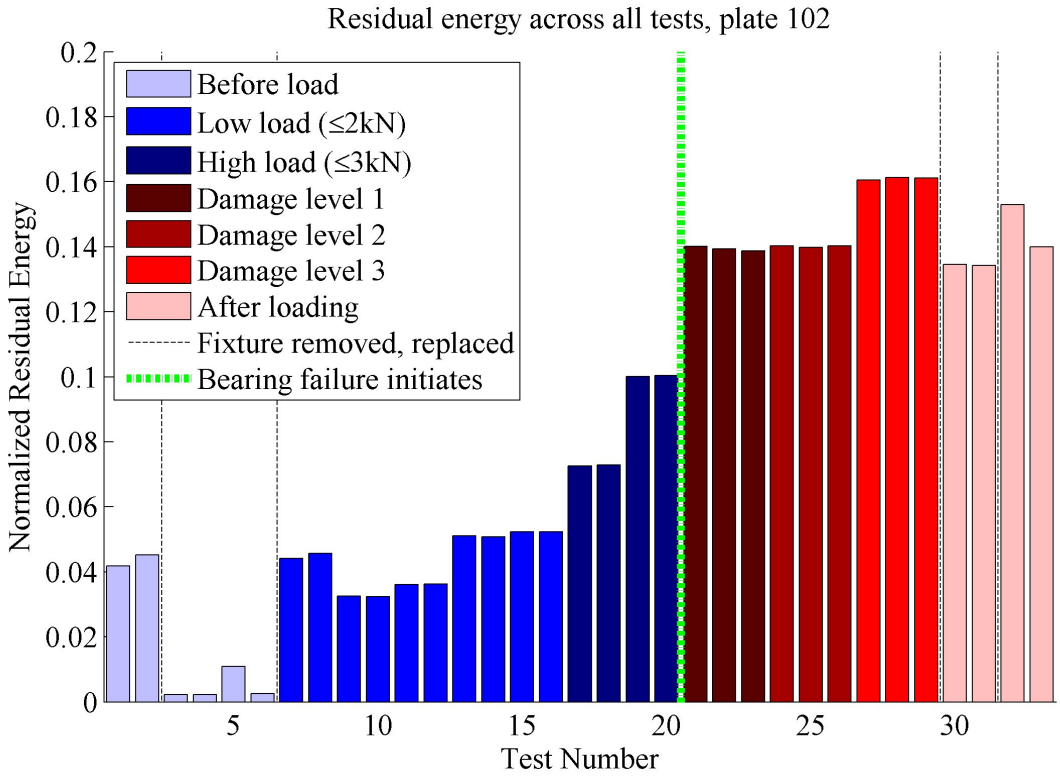

Figure 16 - Normalized residual energy for plate 102 tests. Results shown are for 300 kHz actuation frequency.

Finally, bolt bearing damage appears as a further increase in residual level, which can be detected by appropriate threshold selection according to the usual SHM procedure. To demonstrate the damage detection potential of the system, Figure 16 shows the normalized residual energy for the plate 102 tests. Only the result for 300 kHz is given, but all of the other frequencies showed similar results in that the residual levels for all damaged tests were greater than the undamaged tests. For the example in Figure 16, it is clear that if a threshold level of around 0.12 had been chosen the SHM system would yield 100% correct detection with no false alarms. It should be noted that this comparison is using the data from all eight sensors (considering the average of the normalized residual energy), which would most likely not be the arrangement used for an actual SHM application. However, similar or even better results can be obtained by choosing sensor locations with the information presented in the previous section on optimal interrogation angles. Of course, the case in the field would not be as simple and perfect detection would not be possible in practice, but this result is presented as validation that the approach presented is capable of correctly identifying bolt bearing failure.

CONCLUSION

The ability of a sparse-array UGWSHM system to detect bolt bearing damage in composite structures has been demonstrated in this study. Two specimens were tensile tested, using differing procedures, to introduce the damage in three stages. Both were instrumented with identical circular arrays of MFC sensor-actuators, thereby facilitating a scattering matrix interpretation of the results. Even though sensor-to-sensor variability hinders a direct comparison to theoretical results, the scattering matrix results demonstrate

that the baseline-subtraction strategy is effective in separating the different damage classes. It was further shown that for an unloaded plate the backscatter angles are most sensitive to bolt bearing damage, whereas when the plate is under tensile load the through-transmission angles are most sensitive, which is an important detail for the design of a potential SHM system for monitoring this type of failure. The effect of actuation frequency was examined, concluding that an appropriate frequency had been selected and that the optimal frequency in this situation seems to be directly related to the resulting signal amplitude. Applied load was determined to be a significant parameter affecting the ultrasonic results, yet one that can be compensated for and monitored conveniently through application of the OBS framework, at least in the uniaxial case; this is one of the key major findings of this work.

With proper normalization schemes as suggested in this work, it would be possible to design "scattering filters" through which test data could be projected to characterize and quantify the bearing failure. Such filters would of course be completely failure-mode-dependent. As better micro-mechanical models of bolt bearing failure become available, it may also be beneficial to generalize the experimental results through simulation of the interaction of guided waves with this damage mode. More complex loading conditions and the interaction of temperature changes with load changes would cause corresponding increases in the complexity of the OBS framework – more study may be necessary to achieve effective environmental compensation in such situations. Finally, it would be beneficial to carry out further studies using embeddable sensors (a major focus of aerospace SHM research currently) as well as for more complicated geometries and layups to confirm that the approach remains viable as system complexity increases.

ACKNOWLEDGMENTS

This work was supported jointly by the National Science Foundation (under Grant No. 1207615) and the Japan Society for the Promotion of Science through an East Asia & Pacific Summer Institutes Fellowship (Colin Haynes) as well as by the National Science Foundation through a Graduate Research Fellowship (Colin Haynes). This study was also partially performed under a research grant (No. UD120027JD) supported by the Agency for Defense Development of the Korean government and this paper was also supported by Leading Foreign Research Institute Recruitment Program (2011-0030065) of the National Research Foundation (NRF) of Korea funded by the Ministry of Education, Science and Technology. The authors gratefully acknowledge the hospitality and assistance of the members of the Smart Composites System Laboratory and the Production Technology Research Group at the University of Tokyo. From the Structural Health Monitoring Group at UC San Diego, Richard Do contributed to this work.

REFERENCES

1. Camanho PP, Lambert M. (2006). "A design methodology for mechanically fastened joints in laminated composite materials." *Composites Science and Technology*. 66(15): 3004–3020.

2. Thoppul SD, Finegan J, Gibson RF. (2009). "Mechanics of mechanically fastened joints in polymer–matrix composite structures – A review." *Composites Science and Technology*. 69(3–4): 301–329.

3. Nadabe T, Nishikawa M, Nakamura T, Takeda N. (2009). "Damage Evolution Mechanism in Bolted Joints of CFRP Laminates." *Proc. 24th ASC Technical Conference*. 174–187. Delaware.

4. Xiao Y, Ishikawa T. (2005). "Bearing strength and failure behavior of bolted composite joints (part I: Experimental investigation)." *Composites Science and Technology*. 65(7–8): 1022–1031.

5. Croxford AJ, Wilcox PD, Drinkwater BW, Konstantinidis G. (2007). "Strategies for guided-wave structural health monitoring." *Proceedings of the Royal Society A: Mathematical, Physical and Engineering Science*. 463(2087): 2961–2981.

6. Doyle D, Zagrai A, Arritt B, Çakan H. (2010). "Damage Detection in Bolted Space Structures." *Journal of Intelligent Material Systems and Structures*. 21(3): 251–264.

7. Zagrai A, Gigineishvili V, Kruse WA, Murray A, Doyle D, Reynolds W, et al. (2010). "Acousto-elastic measurements and baseline-free assessment of bolted joints using guided waves in space structures." *Proc. Proc. SPIE*. 765017. San Diego, CA.

8. Lee SJ, Gandhi N, Michaels JE, Michaels TE. (2011). "Comparison of the Effects of Applied Loads and Temperature Variations on Guided Wave Propagation." *AIP Conference Proceedings*. 1335(1): 175–182.

9. Chen X, Michaels JE, Lee SJ, Michaels TE. (2012). "Load-differential imaging for detection and localization of fatigue cracks using Lamb waves." *NDT & E International*. 51: 142–149.

10. Jhang K-Y, Quan H-H, Ha J, Kim N-Y. (2006). "Estimation of clamping force in high-tension bolts through ultrasonic velocity measurement." *Ultrasonics*. 44, Supplement: e1339–e1342.

11. Lanza di Scalea F, Matt H, Bartoli I, Coccia S, Park G, Farrar C. (2007). "Health Monitoring of UAV Wing Skin-to-spar Joints using Guided Waves and Macro Fiber Composite Transducers." *Journal of Intelligent Material Systems and Structures*. 18(4): 373–388.

12. Okabe Y, Fujibayashi K, Shimazaki M, Soejima H. (2011). "Damage Detection in Aircraft Composite Materials Using a Built-in Broadband Ultrasonic Propagation System." *Journal of System Design and Dynamics*. 5(5): 966–981.

13. Wilcox PD, Velichko A. (2010). "Efficient frequency-domain finite element modeling of two-dimensional elastodynamic scattering." *Journal of the Acoustical Society of America*. 127(1): 155–165.

14. Collet M, Ruzzene M, Cunefare KA. (2011). "Generation of Lamb waves through surface mounted macro-fiber composite transducers." *Smart Materials and Structures*. 20(2): 025020.

15. Haynes C, Todd MD, Flynn E, Croxford A. (2012). "Statistically-based damage detection in geometrically-complex structures using ultrasonic interrogation." *Structural Health Monitoring*.

16. Sun H-T, Chang F-K, Qing X. (2002). "The Response of Composite Joints with Bolt-Clamping Loads, Part II: Model Verification." *Journal of Composite Materials*. 36(1): 69–92.

17. Croxford AJ, Moll J, Wilcox PD, Michaels JE. (2010). "Efficient temperature compensation strategies for guided wave structural health monitoring." *Ultrasonics*. 50(4-5): 517–528.

18. Zhang J, Drinkwater B, Wilcox P. (2008). "Defect characterization using an ultrasonic array to measure the scattering coefficient matrix." *Ultrasonics, Ferroelectrics and Frequency Control, IEEE Transactions on*. 55(10): 2254 –2265.

19. Haynes C, Nadabe T, Takeda N, Todd M. (2012). "Scattering Matrix Approach to Informing Damage Monitoring and Prognosis in Composite Bolted Connections." *Proc. Asia-Pacific Workshop on Structural Health Monitoring*. Melbourne, Australia.

20. Fromme P, Sayir MB. (2002). "Measurement of the scattering of a Lamb wave by a through hole in a plate." *The Journal of the Acoustical Society of America*. 111(3): 1165–1170.

21. Salas KI, Cesnik CES. (2010). "Guided wave structural health monitoring using CLoVER transducers in composite materials." *Smart Mater. Struct.* 19(1): 015014.

22. Prosser WH. (1987). *Ultrasonic Characterization of the Nonlinear Elastic Properties of Unidirectional Graphite/Epoxy Composites.* NASA Langley Research Center.

23. Haynes C, Todd M. (2013). "Effect of Applied Load on Guided Wave Monitoring of a Composite Bolted Joint." *Proc. International Workshop on Structural Health Monitoring 2013*. Stanford University.